GSurf: 3D Reconstruction via Signed Distance Fields with Direct Gaussian Supervision

Baixin Xu[1*] Jiangbei Hu[2] Jiaze Li[1] Ying He[1†]
[1] Nanyang Technological Univerisy [2] Dalian University of Technology

Abstract

Surface reconstruction from multi-view images is a core challenge in 3D vision. Recent studies have explored signed distance fields (SDF) within Neural Radiance Fields (NeRF) to achieve high-fidelity surface reconstructions. However, these approaches often suffer from slow training and rendering speeds compared to 3D Gaussian splatting (3DGS). Current state-of-the-art techniques attempt to fuse depth information to extract geometry from 3DGS, but frequently result in incomplete reconstructions and fragmented surfaces. In this paper, we introduce GSurf, a novel end-to-end method for learning a signed distance field directly from Gaussian primitives. The continuous and smooth nature of SDF addresses common issues in the 3DGS family, such as holes resulting from noisy or missing depth data. By using Gaussian splatting for rendering, GSurf avoids the redundant volume rendering typically required in other GS and SDF integrations. Consequently, GSurf achieves faster training and rendering speeds while delivering 3D reconstruction quality comparable to neural implicit surface methods, such as VolSDF and NeuS. Experimental results across various benchmark datasets demonstrate the effectiveness of our method in producing high-fidelity 3D reconstructions.

1. Introduction

Reconstructing high-quality 3D geometry from multi-view images is a central problem in 3D vision, essential for applications such as virtual reality, robotics, and animation, among others. Neural Radiance Fields (NeRF) [36] have demonstrated impressive performance in novel view synthesis by combining implicit representations [35, 39, 41] with volume rendering. Numerous NeRF variants have extended its applications to geometry reconstruction [47, 63], inverse rendering [12, 21, 22, 69, 72], editing [1, 45, 60, 66], and generation [5, 6]. However, these NeRF-based approaches encounter limitations in training and rendering efficiency due to the computational demands of implicit representations coupled with volume rendering. To address these limitations, explicit 3D supervision and discrete representations, such as point-based methods [10, 67, 73], have been introduced to improve efficiency. By transitioning from implicit to discrete representations, these approaches aim to reduce computational demands without compromising reconstruction quality. In this context, 3D Gaussian Splatting (3DGS) [25] introduces a discrete representation with CUDA-based rasterization, significantly reducing training times to minutes and enabling real-time rendering. Beyond novel view synthesis, 3DGS also enhances surface reconstruction. A popular way for obtaining 3D geometry from 3DGS is to extract meshes by fusing rendered depth maps. This approach can achieve high-resolution geometry, but it often lacks robustness, leading to inconsistencies across different views and producing artifacts in regions with insufficient depth information. Another approach is to train an SDF network in conjunction with a volume rendering branch [8, 64]. Despite the improved geometry quality, incorporating volume rendering with Gaussian splatting introduces redundancy in the differentiable rendering pipeline, resulting in extended training times, ranging from 2 hours [64] to as much as 16 hours [8].

In this paper, we introduce a novel reconstruction method that combines Signed Distance Fields (SDF), a continuous representation, with 3D Gaussians, a discrete representation, achieving a balance between the accuracy of implicit representations and the computational efficiency of explicit ones. Specifically, we train the SDF directly under Gaussian supervision, eliminating the need for volume rendering and thereby maintaining high training efficiency. To improve the alignment of Gaussians with the surface, we regularize opacity using an entropy-based loss, which effectively reduces redundant transparent Gaussians. Additionally, we incorporate an MLP to integrate geometry cues–such as normals and geometric features–into the appearance modeling, moving beyond a sole reliance on spherical harmonics. This approach greatly enhances geometric detail compared to existing GS-based reconstruction meth-

[*] Project page: https://github.com/xubaixinxbx/Gsurf.
[†] Corresponding author: Y. He (yhe@ntu.edu.sg).

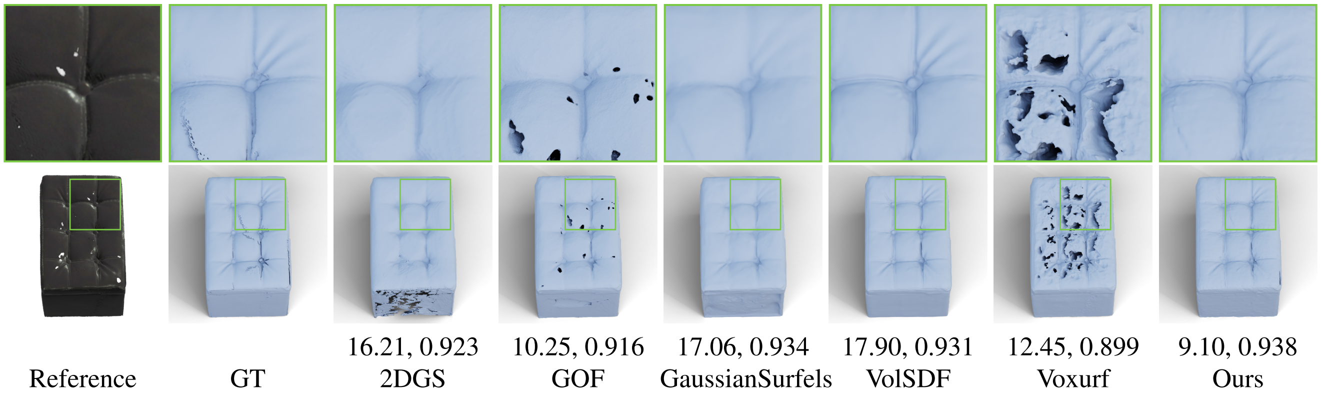

Figure 1. GSurf learns a signed distance field directly from Gaussian primitives. By using Gaussian splatting for rendering, it avoids the redundant volume rendering typically required in other GS and SDF integrations. As a result, GSurf achieves faster training and rendering speeds than previous methods integrating Gaussian splatting with SDF. Our method also exhibits enhanced reconstruction quality compared to neural implicit surface methods, such as VolSDF [63] and Voxurf [56], and state-of-the-art GS-based reconstruction techniques such as 2DGS [19], GOF [65] and GaussianSurfels [11], and neural implicit surface techniques such as VolSDF [63] and Voxurf [56], especially for models under strong lighting conditions. Chamfer distance ($\times 10^3 \downarrow$) and normal consistency ($\uparrow$) are reported as accuracy metrics for each method. Note that CD can be misleading as it may include boundaries or unseen parts of the mesh from multi-view images, such as the underside of the sofa, while NC is more aligned with human perception of quality.

ods. Fig. 1 shows an example of reconstructed surfaces by our method and state-of-the-art approaches.

In summary, this paper makes the following contributions:

- We propose a novel method that simultaneously trains Gaussians and SDF, with direct supervision from Gaussian positions.
- Through the introduction of an entropy-based loss for Gaussian opacity, our method effectively reduces the influence of transparent Gaussians, which can otherwise adversely affect SDF learning.
- By incorporating normals and geometric features into appearance modeling, our method achieves significantly enhanced geometric detail compared to existing approaches.

2. Related works

Point cloud reconstruction with implicit representations. Reconstructing 3D surfaces from point clouds is a fundamental problem in computer graphics that has been extensively studied over the past three decades. Classic approaches typically formulate this problem by computing an implicit function, where a level set at a specified iso-value represents the target surface [17, 18, 23, 24, 31, 38, 61]. In recent years, with the rise of 3D deep learning, combing implicit functions–especially signed distance fields [3, 39, 44, 48, 53]–with deep neural networks has become a mainstream approach. Common methods for regularizing SDFs include the Eikonal loss [15], the neural pull loss [2], and the singular Hessian loss [54].

Multi-view 3D reconstruction. Two seminal works, NeuS [47] and VolSDF [63], enable volume rendering with SDFs by modeling volume density from signed distance. Leveraging the continuous and smooth representations of SDF, these methods demonstrate significantly improved reconstruction quality compared to density-based methods [36]. They have inspired numerous follow-up works aimed at improving runtime performance [14, 50], enhancing reconstruction detail [49], and addressing robustness issues in sparse-view reconstructions [32, 59], among others. To reduce the high computational demands of volume rendering, recent trends have focused on hybrid structures, such as regular grids [13, 46, 56], octrees [28, 29], triplanes [6, 51], hash grids [30, 37, 40, 52], which are combined with or used as replacements for the MLP in NeRF [36].

Surface reconstruction with 3D Gaussians. 3D Gaussian Splatting [25] was introduced for novel view synthesis, enabling real-time rendering and efficient training through CUDA-based rasterization, outperforming earlier volume-rendering methods. However, 3DGS does not specifically address geometry reconstruction. To tackle this, 2D Gaussian Splatting (2DGS) [19] represents scenes using a set of flat 2D disk primitives that align more closely with surfaces. Most current approaches focus on improving the depth accuracy rendered by Gaussians [7, 9, 55, 70]. After training Gaussians, these methods often use depth fusion from off-shell points to extract meshes via a truncated signed distance function (TSDF). Alternatively, SuGaR[16] and GSurfels [11] apply Poisson surface reconstruction [23, 24] to generate meshes. However, meshes derived from depth maps frequently suffer from issues such as holes, lack of smoothness, and incompleteness. Furthermore, the geometry produced by these methods cannot be effectively used to guide the training of Gaussians. Gaussian opacity fields (GOF) [65] enable direct geometry extraction from 3D Gaussians by identifying its level set, without resorting to Poisson reconstruction or TSDF fusion as in previous work.

Other works, such as [34, 58, 64], incorporate SDF into the Gaussian rendering pipeline and use Marching Cubes [33] to extract meshes, effectively addressing issues of holes and achieving smooth, complete geometry. However, in addition to Gaussian splatting for rendering, these approaches also rely on volume rendering, which introduces redundant dual rendering steps, increasing training time and reducing the efficiency of Gaussian splatting. GS-Pull [71], a concurrent work, treats Gaussians as point clouds and pulls query points toward the zero-level set of a learned SDF using its gradient. GS-Pull often produces over-smoothed reconstructions, losing fine details. In contrast, our method integrates geometric cues directly into appearance modeling, eliminating the need for pull operations and yielding in more detailed and accurate geometry.

3. Method

3.1. Overview

Given a set of posed multi-view RGB images, denoted as $\mathcal{I}$, our objective is to reconstruct the following components:

- A set of Gaussian primitives (Sec. 3.2), each characterized by opacity, scale, and rotation, collectively defining the object in a discrete manner;
- A signed distance field (Sec. 3.3), which defines the object's geometry in a continuous manner; and
- An appearance field (Sec. 3.5), which represents the object's radiance.

Both the signed distance field and the appearance field are parameterized using MLPs. In the original 3DGS rendering pipeline, Gaussian primitives are not required to lie exactly on the surface, and off-surface primitives, which are (semi-)transparent, can still contribute to rendering. While these off-surface primitives are acceptable for rendering purposes, they can adversely affect 3D reconstruction and may introduce significant distortions in the reconstructed surface. Therefore, a primary goal in GSurf is to minimize these off-surface primitives. To achieve this, we regularize the Gaussian primitives using an opacity entropy loss (Sec. 3.4), encouraging their opacities to approach one and limiting transparent Gaussian primitives. Fig. 2 illustrates the algorithmic pipeline of GSurf, with technical details provided in the following subsections.

3.2. Gaussian splatting

We adopt 2DGS [19] for rendering, which represents 3D objects with a set of 2D Gaussian primitives (i.e., elliptical disks). Each primitive is parameterized by a central position $\mathbf{p}_k \in \mathbb{R}^3$, two principal tangent vectors $\mathbf{t}_u, \mathbf{t}_v \in \mathbb{R}^3$, and two scaling factors $s_u, s_v \in \mathbb{R}$. Let $\mathbf{R}_k = [\mathbf{t}_u, \mathbf{t}_v, \mathbf{t}_u \times \mathbf{t}_v]$ be the rotation matrix, and $\mathbf{S}_k = \mathrm{diag}(s_u, s_v, 0)$ be the diagonal matrix for scaling. This setup defines a 2D Gaussian within a local tangent plane in the world coordinate system as:

$$\mathbf{P}(u,v) = \mathbf{p}_k + s_u\mathbf{t}_u u + s_v\mathbf{t}_v v = \mathbf{H}(u,v,1,1)^T,$$

where

$$\mathbf{H} = \begin{bmatrix} \mathbf{R}_k\mathbf{S}_k & \mathbf{p}_k \\ \mathbf{0} & 1 \end{bmatrix}$$

is a 4×4 transformation matrix. For each point $\mathbf{u} = (u,v)^T$, its 2D Gaussian value is computed using the standard Gaussian formula:

$$\mathcal{G}(\mathbf{u}) = \exp\left(-\frac{u^2+v^2}{2}\right).$$

These 2D Gaussians are then sorted based on the depth of their centers. To render a pixel x, we cast a ray into the scene and accumulate color using volumetric alpha blending as follows:

$$\mathbf{c}(x) = \sum_{i=1} w_i\mathbf{c}_i,$$

where

$$w_i = o_i\mathcal{G}_i\left(\mathbf{u}(x)\right)\prod_{j=1}^{i-1}\left(1 - o_j\mathcal{G}_j(\mathbf{u}(x))\right),$$

and o_i represents the opacity.

Supervised with a color loss L_{rgb}, 2DGS also introduces regularization terms for depth distortion L_{dep} and depth-normal consistency L_{dnc}, formulated as:

$$L_{\text{gs}} = L_{\text{rgb}} + L_{\text{dep}} + L_{\text{dnc}}. \tag{1}$$

We refer the reader to [19] for more details about these terms.

It is important to note that we have made two modifications to 2DGS to tailor it to our task. First, in our setting, the color $\mathbf{c}_i$ is not represented by spherical harmonics (SH) as in vanilla-GS [19, 25]; instead, we use an MLP to predict $\mathbf{c}_i$, as discussed further in Sec. 3.5. Second, we require that the majority of Gaussian disks have high opacity, ensuring they align closely with the surface of the target object. This differs from 2DGS and 3DGS, which typically contain many semi-transparent primitives spread throughout the entire space. We will discuss Gaussian regularization in Sec. 3.4.

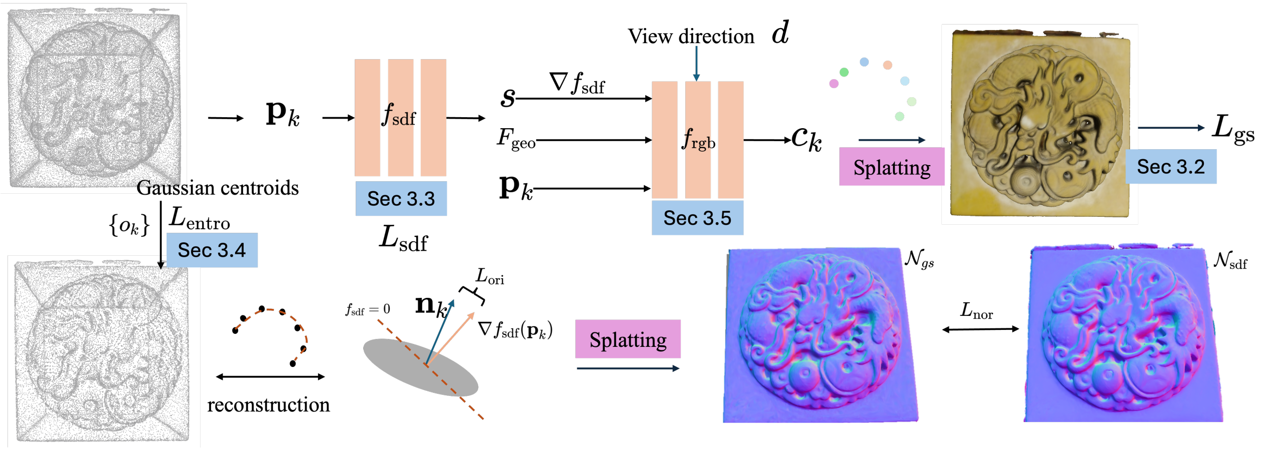

Figure 2. Algorithmic pipeline. Starting from Gaussian centroids, we train a geometry network to learn an SDF (Sec. 3.3) while simultaneously regularizing opacities with an entropy loss (Sec. 3.4). Gaussian positions, normals, geometric features, and viewpoints are then fed into the appearance module to obtain view-dependent colors (Sec. 3.5). Finally, the 3D Gaussians are rasterized into image space to produce images (Sec. 3.2).

3.3. Learning SDF from Gaussians

Inspired by recent advances in shape representation using SDF [3, 39, 44, 48, 53, 54] and the success of SDF-based approaches in NeuS [47] and VolSDF [63], we fit an SDF directly to the Gaussian centroids, which offers several advantages: (1) It enables us to regularize the overall geometry using SDF-based losses, such as the Eikonal loss, addressing common issues like holes and non-smoothness observed in TSDF fusion from depth. (2) The SDF provides an alternative means of guiding Gaussian appearance modeling, whereas TSDF fusion methods rely solely on opacity and SHs and cannot directly impact Gaussian appearance modeling during training.

Unlike NeuS-based methods, which are purely trained from 2D images and lack direct 3D supervision, our approach with Gaussians provides explicit 3D supervision, similar to surface reconstruction from point clouds. Given the central positions of the Gaussians, $\mathbf{p}_k$, as discrete representations of the 3D object, our goal is to learn an SDF parameterized by an MLP f_{sdf}. We impose the following conditions to the SDF: (1) Position constraint: $L_{\text{pos}} = \sum_k |f_{\text{sdf}}(\mathbf{p}_k)|$, which encourages the zero-level set to align with the Gaussians. (2) Eikonal constraint: $L_{\text{eik}} = \|\nabla f_{\text{sdf}} - 1\|_2$, to ensure the smoothness f and mimic a true distance field. (3) Off-surface constraint: $L_{\text{off}} = \sum_k \exp\left(-\alpha|f_{\text{sdf}}(\mathbf{q}_k)|\right)$, applied to query points $\mathbf{q}_k$ that are uniformly sampled in the space. This constraint ensures function values for off-surface points remain relatively large, keeping them away from zero. We set $\alpha = 100$ in our implementation. (4) Orientation constraint: $L_{\text{ori}} = 1 - |\mathbf{n}_k \cdot \nabla f_{\text{sdf}}(\mathbf{p}_k)|$, which enforces alignment between the Gaussian orientation $\mathbf{n}_k$ and the SDF's gradient. Here, $\mathbf{n}_k$ is defined by the shortest axis of the disk. (5) Normal map constraint: $L_{\text{nor}} = 1 - \mathcal{N}_{\text{gs}} \cdot \mathcal{N}_{\text{sdf}}$, which minimizes the discrepancy between the normal maps $\mathcal{N}_{\text{sdf}}$ and $\mathcal{N}_{\text{gs}}$ rendered from the SDF and 2DGS.

Putting it all together, the SDF loss is defined as:

$$L_{\text{sdf}} = \lambda_1 L_{\text{pos}} + \lambda_2 L_{\text{eik}} + \lambda_3 L_{\text{off}} + \lambda_4 L_{\text{ori}} + \lambda_5 L_{\text{nor}}. \quad (2)$$

3.4. Gaussian regularization

As mentioned previously, the color loss alone is insufficient to constrain Gaussian primitives to the object's surface, as semi-transparent Gaussians, which are off the surface, also contribute to splatting. To ensure that all Gaussian centroids are correctly positioned on the surface–a key requirement in learning the SDF that accurately represents surface geometry–we introduce a penalty for Gaussian primitives with low opacities.

In this paper, we focus on opaque objects, and thus we aim for the Gaussians to be as opaque as possible. To achieve this, we introduce a loss function that regularizes the opacity of the Gaussians to converge to either 0 or 1, using an entropy-based approach:

$$L_{\text{ent}} = \lambda_6 \left(-\sum_k o_k \ln(o_k) \right). \quad (3)$$

During the training process, Gaussians with opacities lower than a threshold are eliminated.

3.5. Geometry-guided appearance modeling

As noted in previous works [56, 59], if appearance modeling in volume rendering relies solely on input position and viewpoint, it becomes challenging to capture detailed geometry in reconstruction. A common approach to address this challenge is to incorporate geometric cues, such as normals and geometric features, into the rendering process [62].

Following this approach, in the SDF module, f_{sdf}, besides outputting the signed distance value s, we also obtain a geometric feature F_{geo} for each Gaussian centroid $\mathbf{p}_k$:

$$(s, F_{\text{geo}}) = f_{\text{sdf}}(\mathbf{p}_k). \tag{4}$$

We then feed the appearance module f_{app} with the position $\mathbf{p}_k$, viewing direction $\mathbf{d}$, normals ∇f_{sdf}, and geometry feature F_{geo} as inputs:

$$\mathbf{c}_k = f_{\text{rgb}}\left(\mathbf{p}_k, \mathbf{d}, \nabla f_{\text{sdf}}, \mathrm{F}_{\text{geo}}\right), \tag{5}$$

obtaining the color $\mathbf{c}_k$.

3.6. Implementation details

The overall loss function in GSurf is defined as follows:

$$L_{\text{total}} = L_{\text{gs}} + L_{\text{sdf}} + L_{\text{ent}}. \tag{6}$$

We train GSurf on a single NVIDIA A800 GPU. Following IDR [62], we model the SDF and appearance with MLPs of 8 and 4 layers, respectively, each with 256 hidden units and ReLU activation.

Since 3D Gaussians are initialized randomly rather than with COLMAP [42, 43], which is time consuming, we delay the activation of SDF learning, beginning SDF training only after the first 500 iterations. To promote robust convergence, the SDF is initialized as a sphere. Both the Gaussians and the MLPs are optimized using the Adam optimizer [26].

We adopt the same densification strategies as those used in 2DGS [19]. The hyperparameters are empirically set to $\lambda_1 = 0.1, \lambda_2 = \lambda_3 = \lambda_6 = 0.01$, and $\lambda_4 = \lambda_5 = 0.05$.

4. Experimental results

4.1. Setup

Datasets and metrics. We evaluate our method on the DTU dataset [20], a widely used benchmark for 3D reconstruction. Additionally, we assess performance on two subsets of the OmniObjects3D dataset [57]. OmniObjects3D-d includes categories such as antiques and ornaments, featuring rich geometric details across 8 objects, while OO3D-SL [29] consists of 24 objects under strong lighting conditions, which often pose challenges for 3D reconstruction methods. Each OmniObjects3D object has approximately 100 images with a resolution of 800 × 800 pixels and a groud-truth mesh. Furthermore, we evaluate our method on the α-NeuS dataset [68], which consists of 10 synthetic and real-world (semi-)transparent models. We report Chamfer Distance (CD) as a measure of geometric accuracy. For models in the OmniObjects3D dataset, we also report normal consistency (NC), as ground truth meshes are available. NC performance is typically more aligned with human perception of quality. Evaluation scripts for DTU and OmniObjects3D are sourced from 2DGS [19], GOF [65], and the official OmniObjects3D repository [57].

Baselines. We compare our method with state-of-the-art 3DGS-based reconstruction methods, including 2DGS [19], GOF [65], and GaussianSurfels [11] on the DTU and OmniObjects3D datasets. For GaussianSurfels [11], we observed that its pre-trained normal prediction model often produced incorrect normals (and sometimes completely flipped orientations) on models from the OmniObjects3D dataset. Consequently, we disabled the normal estimation from the pre-trained model in our evaluation on the OmniObjects3D dataset.

4.2. Comparisons

Training times. When trained on a single NVIDIA A800 GPU, our method achieves competitive speeds, with training times ranging from 40 minutes to 1.3 hours, compared to previous methods integrating Gaussian splatting with SDF, which take from 2 hours [64] up to 16 hours [8].

Results on the DTU dataset. As shown in Tab. 1, our method achieves reconstruction results that are comparable to, though not the best among, the baselines. However, we observed that Chamfer Distance should not be used as the sole quality measure for the DTU dataset due to (1) noise and holes in the ground truth point clouds and (2) the cropping process, which may retain boundary regions that contribute to a higher CD. Setting an accurate manual threshold for cropping is challenging. Fig. 3 shows visual results of our method alongside baseline methods for six models. For complete visual results on the DTU dataset, we refer the reader to the supplementary material and accompanying video. Through qualitative comparison, we found that our method better captures fine geometric details and produces smoother surfaces. For instance, on the can's surface in scan 97 (third column in Fig. 3), our method preserves detail even though reflective properties introduce noisy depth in Gaussian splatting.

Results on the OmniObject3D-d dataset. VolSDF [63] requires extensive training time (exceeding 10 hours for each model on the OmniObjects3D dataset) due to the computational demands of volume rendering. As shown in Tab. 2, both 2DGS [19] and GOF [65] exhibit broken surfaces, resulting in poor CD scores. While GaussianSurfels [11] effectively address the issues of holes (e.g., see the second row in Fig. 4), which are common in depth map fusion techniques [19], it requires a significantly larger number of Gaussian primitives compared to our method, as shown in Fig. 4.

Table 1. Quantitative evaluation on the DTU dataset. We compare our method with volume rendering-based and Gaussian splatting-based reconstruction methods using CD (10^3, ↓). The best results are highlighted with 1st, 2nd, and 3rd.

Method	24	37	40	55	63	65	69	83	97	105	106	110	114	118	122	Mean
NeuS [47]	1.00	1.37	0.93	0.43	1.10	0.65	0.57	1.48	1.09	0.83	0.52	1.20	0.35	0.49	0.54	0.84
VolSDF [63]	1.14	1.26	0.81	0.49	1.25	0.70	0.72	1.29	1.18	0.70	0.66	1.08	0.42	0.61	0.55	0.86
3DGS [25]	2.14	1.53	2.08	1.68	3.49	2.21	1.43	2.07	2.22	1.75	1.79	2.55	1.53	1.52	1.50	1.96
2DGS [19]	0.48	0.91	0.39	0.39	1.01	0.83	0.81	1.36	1.27	0.76	0.70	1.40	0.40	0.76	0.52	0.80
GOF [65]	0.50	0.82	0.37	0.37	1.12	0.74	0.73	1.18	1.29	0.68	0.77	0.90	0.42	0.66	0.49	0.74
GSurfels [11]	0.66	0.93	0.54	0.41	1.06	1.14	0.85	1.29	1.53	0.79	0.82	1.58	0.45	0.66	0.53	0.88
Ours	0.52	1.00	0.48	0.47	0.79	1.27	0.82	1.24	1.27	0.65	0.89	1.26	0.52	0.76	0.73	0.84

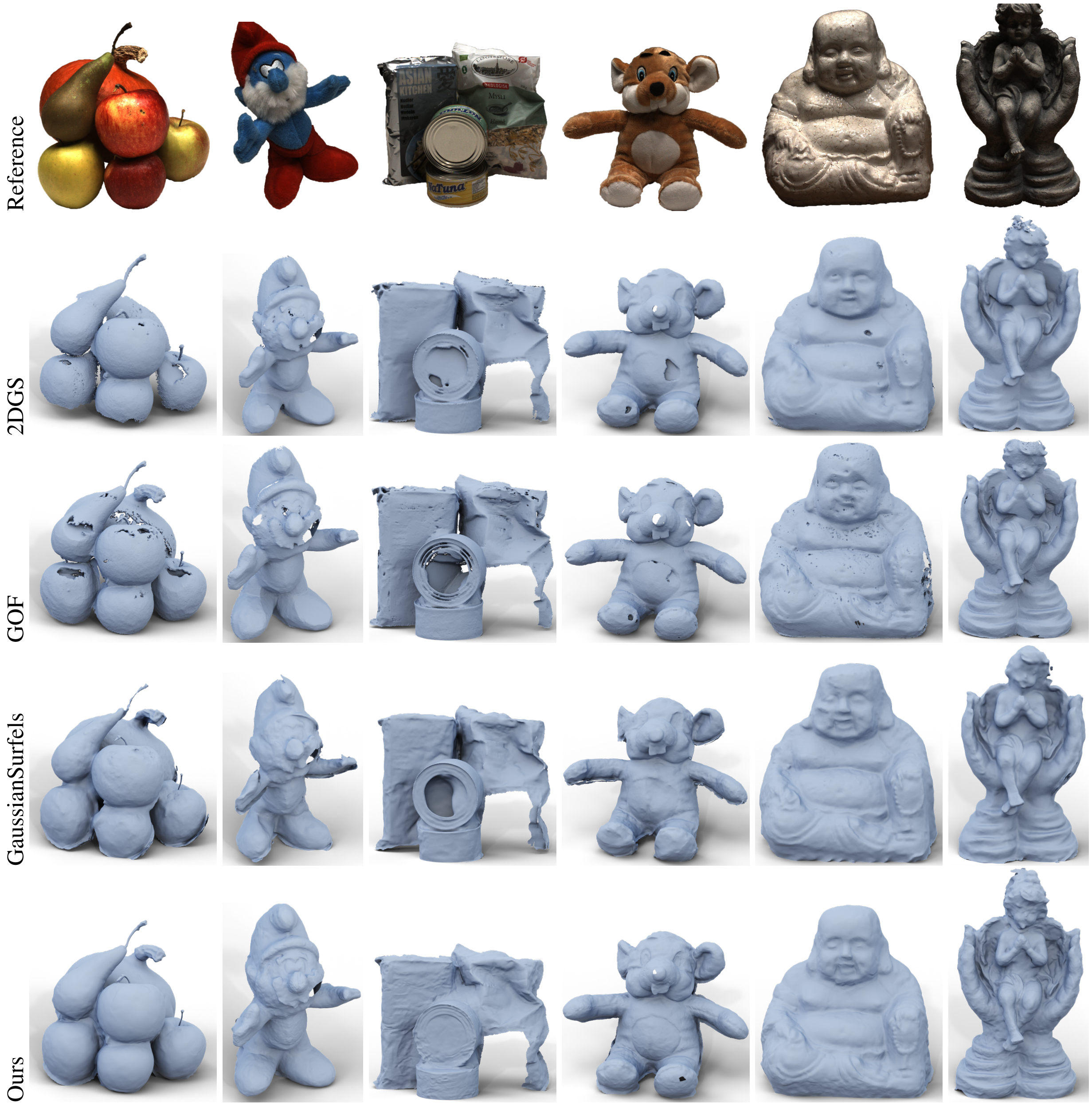

Figure 3. Visual results on the DTU dataset. We present visualizations of the culled meshes after applying cropping, using the scripts from 2DGS [19] and GOF [65].

Table 2. Quantitative evaluation on the OmniObjects3D-d dataset. We report CD ($\times 10^3$ ↓) and Normal Consistency (NC ↑). OR and GAM stand for opacity regularization and geometry-guided appearance modeling, respectively. 2DGS+NSH refers to the integration of Gaussian splatting with NSH [54], a deep learning model for point cloud reconstruction, where the generated Gaussian primitives are fed into the NSH network. The best results (excluding our ablation methods) are highlighted with 1st , 2nd , and 3rd .

Method	Ornaments										Antique					
	1		3		4		5		8		16		19		21	
	CD	NC	CD	NC	CD	NC	CD	NC	CD	NC	CD	NC	CD	NC	CD	NC
VolSDF [63]	12.13	0.950	4.32	0.992	14.00	0.939	9.11	0.959	22.89	0.903	29.45	0.938	11.60	0.906	12.56	0.932
2DGS [19]	8.27	0.954	19.63	0.924	8.74	0.964	5.82	0.962	32.74	0.813	10.86	0.939	11.68	0.853	12.11	0.940
GOF [65]	7.90	0.956	4.66	0.992	12.16	0.961	5.97	0.966	44.08	0.790	23.71	0.898	15.44	0.834	21.76	0.966
GSurfels [11]	11.13	0.950	7.57	0.980	9.55	0.970	8.05	0.962	13.95	0.886	11.84	0.943	9.28	0.918	9.36	0.962
2DGS+NSH [54]	11.26	0.922	12.85	0.936	16.12	0.905	9.68	0.942	11.27	0.893	23.13	0.901	15.37	0.860	33.18	0.873
Ours	7.04	0.959	3.11	0.978	8.34	0.967	6.35	0.960	18.04	0.856	14.99	0.922	8.46	0.882	5.47	0.956
Ours (w/o GAM)	7.83	0.938	6.73	0.964	9.43	0.963	7.46	0.952	20.56	0.812	17.88	0.918	10.43	0.886	5.97	0.962
Ours (w/o OR)	12.50	0.917	25.20	0.920	27.18	0.869	21.92	0.888	27.19	0.831	28.13	0.845	18.83	0.828	13.72	0.924

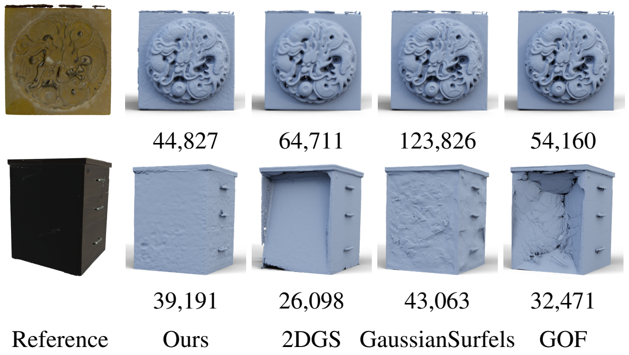

Figure 4. Comparison on the Antique 016 and Table 019 models from the OmniObjects3D dataset. The number of Gaussians used by each method is also reported.

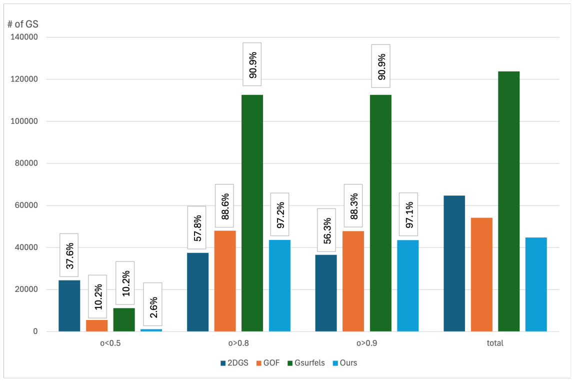

Figure 5. Comparison of Gaussian counts on the Antique 016 model between our method and 2DGS [19], GOF [65], and GaussianSurfels [11]. By applying an entropy loss on opacity, our method effectively reduces the number of Gaussians with low opacity (i.e., semi-transparent Gaussians), ensuring that each generated Gaussian makes a solid contribution to rendering. Consequently, our approach requires fewer Gaussians than existing methods.

We further report the proportion of Gaussians in Fig. 5, showing that 37.6% of Gaussians in 2DGS have opacity values below 0.5. In contrast, our method produces the lowest percentage of transparent Gaussians (2.6%) and maximizes the number of opaque Gaussians, with 97.1% having opacity values greater than 0.9, compared to 56.3% for 2DGS, 88.3% for GOF, and 90.9% for GaussianSurfels. This distribution aligns with our requirements for learning a reliable SDF from Gaussian primitives. GOF [65] filters Gaussians by evaluating their opacity contributions, while GaussianSurfels [11] applies opacity regularization using a bell-shaped exponential function. Our approach achieves the highest ratio of opaque Gaussians, delivering comparable reconstruction performance while maintaining compactness without an excessive number of Gaussians.

Additionally, we compare our method with Neural Singular Hessian (NSH) [54], a state-of-the-art method for learning SDFs from point clouds, applied to Gaussian primitives extracted by 2DGS [19], as shown in Tab. 2. In this approach to integrating SDF with Gaussian splatting, all Gaussian primitives generated by 2DGS are treated as opaque and with fixed positions, and image supervision is not utilized in geometry reconstruction. Consequently, its reconstructed surfaces often exhibit artifacts and lack fine geometric details.

Results on the OO3D-SL and α-NeuS datasets. The OO3D-SL and α-NeuS datasets feature models with strong lighting conditions and (semi-)transparent materials, respectively. We observed that lighting variations have little impact to our method, due to the integration of SDF and Gaussian splatting (see Fig. 1 and Fig. 4). Furthermore, GSurf successfully reconstructs semi-transparent surfaces, as demonstrated in Fig. 7, producing smooth geometry. In contrast, methods based on TSDF fusion [19] or depth-to-3D point conversion with Poisson reconstruction [11] struggle to reconstruct accurate geometry due to unreliable depth information. Our method leverages the smoothness of the

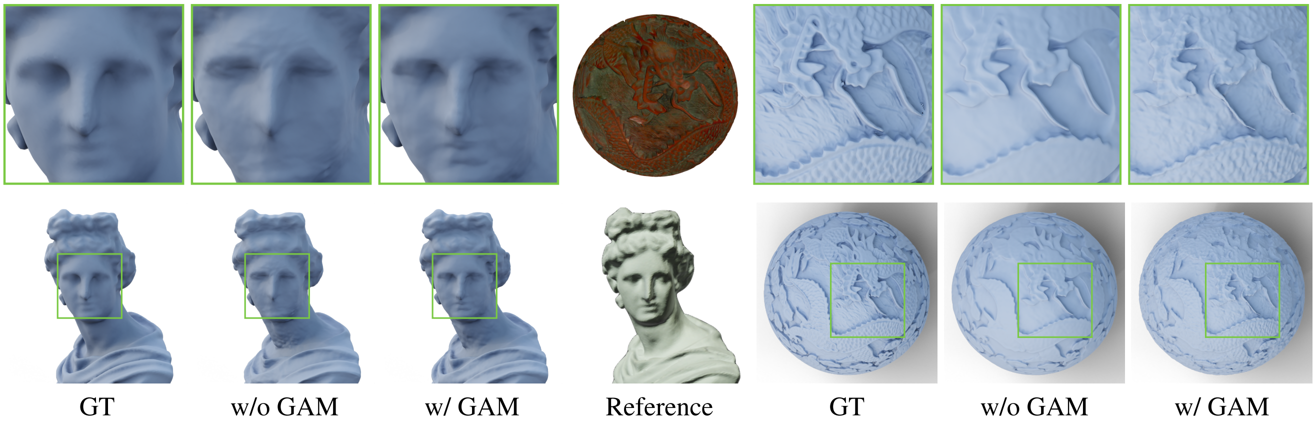

Figure 6. Ablation study on geometry-guided appearance modeling.

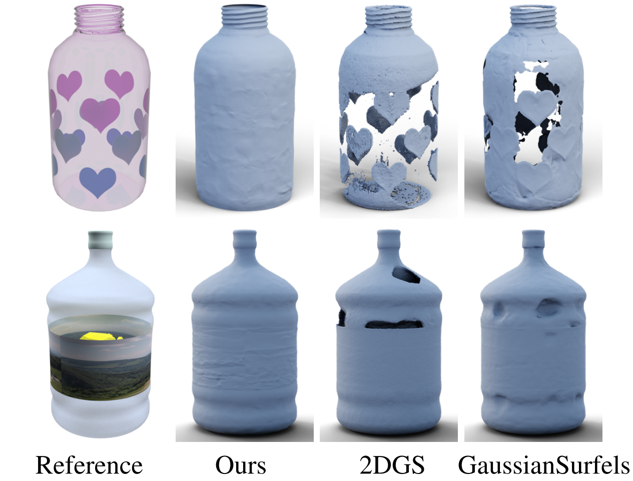

Figure 7. Visual comparison on the α-NeuS dataset for (semi-)transparent objects [68].

SDF under direct supervision of Gaussian primitives, eliminating dependency on potentially unreliable depth maps. In contrast, both TSDF fusion and Poisson reconstruction from depth points face challenges in accurately reconstructing semi-transparent surfaces.

4.3. Ablation studies

Opacity regularization. While low-opacity Gaussians have minimal impact on rendering quality, they significantly disrupt the SDF module, leading to distorted and inaccurate geometries. Therefore, reducing the number of low-opacity Gaussians is crucial for effective integration of SDF and Gaussian splatting. As the quantitative evaluations in Tab. 2 and the ablation study in Tab. 3 show, entropy-based opacity regularization not only reduces the total number of Gaussians but also increases their opacity, aligning them more closely with the zero level set of the SDF.

Table 3. Ablation study on opacity regularization using the Antique 016 model. We report the proportion of Gaussians with opacity o at various thresholds: 0.5, 0.8 and 0.9, respectively.

	$o < 0.5$	$o > 0.8$	$o > 0.9$	Total
w/o OR	39.9%	54.7%	52.8%	58,148
w/ OR	2.6%	97.2%	97.1%	44,827

We observe that when opacity regularization is removed, the Gaussian centroids become unreliable and exhibit slight movement during training, causing instability and noise in the SDF training process. This explains the higher CD observed when Gaussian opacity is not constrained alongside appearance modeling, as shown in Tab. 2.

Geometry-guided appearance modeling. As shown in Tab. 2, omitting geometry features from appearance modeling results in a slight decrease in geometry reconstruction performance. Visual results in Fig. 6 indicate that using spherical harmonics for appearance modeling does not fully capture intricate geometry details. By modeling the object's appearance as a function of geometry features and normals, GSurf improves geometry quality, which in turn enhances rendering quality.

5. Conclusion

This paper introduces GSurf, an end-to-end framework that combines SDF, a continuous representation, with 3D Gaussians, a discrete representation, achieving a balance between the accuracy of implicit representations and the computational efficiency of explicit ones. Unlike existing methods that integrate SDF with volume rendering, our method trains the SDF directly from 3D Gaussians, therefore preserving training efficiency. Experimental results on benchmark datasets demonstrate the effectiveness of GSurf in terms of reconstruction accuracy and rendering quality.

References

[1] Chong Bao, Yinda Zhang, Bangbang Yang, Tianxing Fan, Zesong Yang, Hujun Bao, Guofeng Zhang, and Zhaopeng Cui. Sine: Semantic-driven image-based nerf editing with prior-guided editing field. In *Proceedings of the IEEE/CVF Conference on Computer Vision and Pattern Recognition*, pages 20919–20929, 2023. 1

[2] Ma Baorui, Han Zhizhong, Liu Yu-Shen, and Zwicker Matthias. Neural-pull: Learning signed distance functions from point clouds by learning to pull space onto surfaces. In *International Conference on Machine Learning (ICML)*, 2021. 2

[3] Ma Baorui, Liu Yu-Shen, and Han Zhizhong. Reconstructing surfaces for sparse point clouds with on-surface priors. In *Proceedings of the IEEE/CVF Conference on Computer Vision and Pattern Recognition (CVPR)*, 2022. 2, 4

[4] Jonathan T. Barron, Ben Mildenhall, Dor Verbin, Pratul P. Srinivasan, and Peter Hedman. Mip-nerf 360: Unbounded anti-aliased neural radiance fields. *CVPR*, 2022. 3

[5] Eric R Chan, Marco Monteiro, Petr Kellnhofer, Jiajun Wu, and Gordon Wetzstein. pi-gan: Periodic implicit generative adversarial networks for 3d-aware image synthesis. In *Proceedings of the IEEE/CVF conference on computer vision and pattern recognition*, pages 5799–5809, 2021. 1

[6] Eric R Chan, Connor Z Lin, Matthew A Chan, Koki Nagano, Boxiao Pan, Shalini De Mello, Orazio Gallo, Leonidas J Guibas, Jonathan Tremblay, Sameh Khamis, et al. Efficient geometry-aware 3d generative adversarial networks. In *Proceedings of the IEEE/CVF conference on computer vision and pattern recognition*, pages 16123–16133, 2022. 1, 2

[7] Danpeng Chen, Hai Li, Weicai Ye, Yifan Wang, Weijian Xie, Shangjin Zhai, Nan Wang, Haomin Liu, Hujun Bao, and Guofeng Zhang. Pgsr: Planar-based gaussian splatting for efficient and high-fidelity surface reconstruction. *arXiv preprint arXiv:2406.06521*, 2024. 2

[8] Hanlin Chen, Chen Li, and Gim Hee Lee. Neusg: Neural implicit surface reconstruction with 3d gaussian splatting guidance. *arXiv preprint arXiv:2312.00846*, 2023. 1, 5

[9] Hanlin Chen, Fangyin Wei, Chen Li, Tianxin Huang, Yunsong Wang, and Gim Hee Lee. Vcr-gaus: View consistent depth-normal regularizer for gaussian surface reconstruction. *arXiv preprint arXiv:2406.05774*, 2024. 2

[10] Zhang Chen, Zhong Li, Liangchen Song, Lele Chen, Jingyi Yu, Junsong Yuan, and Yi Xu. Neurbf: A neural fields representation with adaptive radial basis functions. In *Proceedings of the IEEE/CVF International Conference on Computer Vision (ICCV)*, pages 4182–4194, 2023. 1

[11] Pinxuan Dai, Jiamin Xu, Wenxiang Xie, Xinguo Liu, Huamin Wang, and Weiwei Xu. High-quality surface reconstruction using gaussian surfels. In *ACM SIGGRAPH 2024 Conference Papers*, pages 1–11, 2024. 2, 5, 6, 7, 1

[12] Yuxin Dai, Qi Wang, Jingsen Zhu, Dianbing Xi, Yuchi Huo, Chen Qian, and Ying He. Mirres: Multi-bounce inverse rendering using reservoir sampling. *arXiv preprint arXiv:2406.16360*, 2024. 1

[13] Sara Fridovich-Keil, Alex Yu, Matthew Tancik, Qinhong Chen, Benjamin Recht, and Angjoo Kanazawa. Plenoxels: Radiance fields without neural networks. In *Proceedings of the IEEE/CVF conference on computer vision and pattern recognition*, pages 5501–5510, 2022. 2

[14] Qiancheng Fu, Qingshan Xu, Yew Soon Ong, and Wenbing Tao. Geo-neus: Geometry-consistent neural implicit surfaces learning for multi-view reconstruction. In *Advances in Neural Information Processing Systems*, pages 3403–3416, 2022. 2

[15] Amos Gropp, Lior Yariv, Niv Haim, Matan Atzmon, and Yaron Lipman. Implicit geometric regularization for learning shapes. In *Proceedings of Machine Learning and Systems 2020*, pages 3569–3579. 2020. 2

[16] Antoine Guédon and Vincent Lepetit. Sugar: Surface-aligned gaussian splatting for efficient 3d mesh reconstruction and high-quality mesh rendering. In *Proceedings of the IEEE/CVF Conference on Computer Vision and Pattern Recognition*, pages 5354–5363, 2024. 2

[17] Hugues Hoppe, Tony DeRose, Tom Duchamp, John McDonald, and Werner Stuetzle. Surface reconstruction from unorganized points. In *Proceedings of the 19th Annual Conference on Computer Graphics and Interactive Techniques*, page 71–78, New York, NY, USA, 1992. 2

[18] Fei Hou, Chiyu Wang, Wencheng Wang, Hong Qin, Chen Qian, and Ying He. Iterative poisson surface reconstruction (ipsr) for unoriented points. *ACM Trans. Graph.*, 41 (4), 2022. 2

[19] Binbin Huang, Zehao Yu, Anpei Chen, Andreas Geiger, and Shenghua Gao. 2d gaussian splatting for geometrically accurate radiance fields. In *ACM SIGGRAPH 2024 Conference Papers*, pages 1–11, 2024. 2, 3, 5, 6, 7

[20] Rasmus Jensen, Anders Dahl, George Vogiatzis, Engil Tola, and Henrik Aanæs. Large scale multi-view stereopsis evaluation. In *2014 IEEE Conference on Computer Vision and Pattern Recognition*, pages 406–413. IEEE, 2014. 5, 1

[21] Daisheng Jin, Jiangbei Hu, Baixin Xu, Yuxin Dai, Chen Qian, and Ying He. Robust geometry and reflectance disentanglement for 3d face reconstruction from sparse-view images. *arXiv preprint arXiv:2312.06085*, 2023. 1

[22] Haian Jin, Isabella Liu, Peijia Xu, Xiaoshuai Zhang, Songfang Han, Sai Bi, Xiaowei Zhou, Zexiang Xu, and Hao Su. Tensoir: Tensorial inverse rendering. In *Proceedings of the IEEE/CVF Conference on Computer Vision and Pattern Recognition*, pages 165–174, 2023. 1

[23] Michael Kazhdan and Hugues Hoppe. Screened poisson surface reconstruction. *ACM Transactions on Graphics (ToG)*, 32(3):1–13, 2013. 2

[24] Michael Kazhdan, Matthew Bolitho, and Hugues Hoppe. Poisson surface reconstruction. In *Proceedings of the fourth Eurographics symposium on Geometry processing*, 2006. 2

[25] Bernhard Kerbl, Georgios Kopanas, Thomas Leimkühler, and George Drettakis. 3d gaussian splatting for real-time radiance field rendering. *ACM Trans. Graph.*, 42(4):139–1, 2023. 1, 2, 3, 6

[26] Diederik P Kingma. Adam: A method for stochastic optimization. *arXiv preprint arXiv:1412.6980*, 2014. 5

[27] Arno Knapitsch, Jaesik Park, Qian-Yi Zhou, and Vladlen Koltun. Tanks and temples: Benchmarking large-scale scene

reconstruction. *ACM Transactions on Graphics (ToG)*, 36 (4):1–13, 2017. 3

[28] J. Li, Z. Wen, L. Zhang, J. Hu, F. Hou, Z. Zhang, and Y. He. Gs-octree: Octree-based 3d gaussian splatting for robust object-level 3d reconstruction under strong lighting. *Computer Graphics Forum*, 2024. 2

[29] Jiaze Li, Luo Zhang, Jiangbei Hu, Zhebin Zhang, Hongyu Sun, Gaochao Song, and Ying He. Real-time volume rendering with octree-based implicit surface representation. *Computer Aided Geometric Design*, 111:102322, 2024. 2, 5

[30] Zhaoshuo Li, Thomas Müller, Alex Evans, Russell H Taylor, Mathias Unberath, Ming-Yu Liu, and Chen-Hsuan Lin. Neuralangelo: High-fidelity neural surface reconstruction. In *Proceedings of the IEEE/CVF Conference on Computer Vision and Pattern Recognition*, pages 8456–8465, 2023. 2

[31] Siyou Lin, Dong Xiao, Zuoqiang Shi, and Bin Wang. Surface reconstruction from point clouds without normals by parametrizing the gauss formula. *ACM Trans. Graph.*, 42 (2), 2022. 2

[32] Xiaoxiao Long, Cheng Lin, Peng Wang, Taku Komura, and Wenping Wang. Sparseneus: Fast generalizable neural surface reconstruction from sparse views. In *European Conference on Computer Vision (ECCV)*, pages 210–227, 2022. 2

[33] William E Lorensen and Harvey E Cline. Marching cubes: A high resolution 3d surface construction algorithm. In *Seminal graphics: pioneering efforts that shaped the field*, pages 347–353. 1998. 3

[34] Xiaoyang Lyu, Yang-Tian Sun, Yi-Hua Huang, Xiuzhe Wu, Ziyi Yang, Yilun Chen, Jiangmiao Pang, and Xiaojuan Qi. 3dgsr: Implicit surface reconstruction with 3d gaussian splatting. *arXiv preprint arXiv:2404.00409*, 2024. 3

[35] Lars Mescheder, Michael Oechsle, Michael Niemeyer, Sebastian Nowozin, and Andreas Geiger. Occupancy networks: Learning 3d reconstruction in function space. In *Proceedings of the IEEE/CVF conference on computer vision and pattern recognition*, pages 4460–4470, 2019. 1

[36] Ben Mildenhall, Pratul P Srinivasan, Matthew Tancik, Jonathan T Barron, Ravi Ramamoorthi, and Ren Ng. Nerf: Representing scenes as neural radiance fields for view synthesis. *Communications of the ACM*, 65(1):99–106, 2021. 1, 2

[37] Thomas Müller, Alex Evans, Christoph Schied, and Alexander Keller. Instant neural graphics primitives with a multiresolution hash encoding. *ACM Trans. Graph.*, 41(4):102:1–102:15, 2022. 2

[38] Yutaka Ohtake, Alexander Belyaev, Marc Alexa, Greg Turk, and Hans-Peter Seidel. Multi-level partition of unity implicits. *ACM Trans. Graph.*, 22(3):463–470, 2003. 2

[39] Jeong Joon Park, Peter Florence, Julian Straub, Richard Newcombe, and Steven Lovegrove. Deepsdf: Learning continuous signed distance functions for shape representation. In *Proceedings of the IEEE/CVF conference on computer vision and pattern recognition*, pages 165–174, 2019. 1, 2, 4

[40] Christian Reiser, Stephan Garbin, Pratul Srinivasan, Dor Verbin, Richard Szeliski, Ben Mildenhall, Jonathan Barron, Peter Hedman, and Andreas Geiger. Binary opacity grids: Capturing fine geometric detail for mesh-based view synthesis. *ACM Transactions on Graphics (TOG)*, 43(4):1–14, 2024. 2

[41] Shunsuke Saito, Zeng Huang, Ryota Natsume, Shigeo Morishima, Angjoo Kanazawa, and Hao Li. Pifu: Pixel-aligned implicit function for high-resolution clothed human digitization. In *Proceedings of the IEEE/CVF international conference on computer vision*, pages 2304–2314, 2019. 1

[42] Johannes Lutz Schönberger and Jan-Michael Frahm. Structure-from-motion revisited. In *Conference on Computer Vision and Pattern Recognition (CVPR)*, 2016. 5

[43] Johannes Lutz Schönberger, Enliang Zheng, Marc Pollefeys, and Jan-Michael Frahm. Pixelwise view selection for unstructured multi-view stereo. In *European Conference on Computer Vision (ECCV)*, 2016. 5

[44] Liu Shi-Lin, Guo Hao-Xiang, Pan Hao, Peng-Shuai Wang, Tong Xin, and Liu Yang. Deep implicit moving least-squares functions for 3d reconstruction. In *IEEE/CVF Conference on Computer Vision and Pattern Recognition*, 2021. 2, 4

[45] Pratul P Srinivasan, Stephan J Garbin, Dor Verbin, Jonathan T Barron, and Ben Mildenhall. Nuvo: Neural uv mapping for unruly 3d representations. In *European Conference on Computer Vision*, pages 18–34. Springer, 2025. 1

[46] Cheng Sun, Min Sun, and Hwann-Tzong Chen. Direct voxel grid optimization: Super-fast convergence for radiance fields reconstruction. In *Proceedings of the IEEE/CVF conference on computer vision and pattern recognition*, pages 5459–5469, 2022. 2

[47] Peng Wang, Lingjie Liu, Yuan Liu, Christian Theobalt, Taku Komura, and Wenping Wang. Neus: Learning neural implicit surfaces by volume rendering for multi-view reconstruction. In *Advances in Neural Information Processing Systems*, pages 27171–27183, 2021. 1, 2, 4, 6

[48] Peng-Shuai Wang, Yang Liu, and Xin Tong. Dual octree graph networks for learning adaptive volumetric shape representations. *ACM Transactions on Graphics*, 41(4):1–15, 2022. 2, 4

[49] Yiqun Wang, Ivan Skorokhodov, and Peter Wonka. Hf-neus: Improved surface reconstruction using high-frequency details. *Advances in Neural Information Processing Systems*, 35:1966–1978, 2022. 2

[50] Yiming Wang, Qin Han, Marc Habermann, Kostas Daniilidis, Christian Theobalt, and Lingjie Liu. Neus2: Fast learning of neural implicit surfaces for multi-view reconstruction. In *Proceedings of the IEEE/CVF International Conference on Computer Vision (ICCV)*, 2023. 2

[51] Yiqun Wang, Ivan Skorokhodov, and Peter Wonka. Pet-neus: Positional encoding tri-planes for neural surfaces. In *Proceedings of the IEEE/CVF Conference on Computer Vision and Pattern Recognition*, pages 12598–12607, 2023. 2

[52] Zian Wang, Tianchang Shen, Merlin Nimier-David, Nicholas Sharp, Jun Gao, Alexander Keller, Sanja Fidler, Thomas Müller, and Zan Gojcic. Adaptive shells for efficient neural radiance field rendering. *arXiv preprint arXiv:2311.10091*, 2023. 2

[53] Zixiong Wang, Pengfei Wang, Pengshuai Wang, Qiujie Dong, Junjie Gao, Shuangmin Chen, Shiqing Xin, Changhe Tu, and Wenping Wang. Neural-imls: Self-supervised implicit moving least-squares network for surface reconstruction. *IEEE Transactions on Visualization and Computer Graphics*, pages 1–16, 2023. 2, 4

[54] Zixiong Wang, Yunxiao Zhang, Rui Xu, Fan Zhang, Peng-Shuai Wang, Shuangmin Chen, Shiqing Xin, Wenping Wang, and Changhe Tu. Neural-singular-hessian: Implicit neural representation of unoriented point clouds by enforcing singular hessian. *ACM Transactions on Graphics (TOG)*, 42 (6):1–14, 2023. 2, 4, 7

[55] Yaniv Wolf, Amit Bracha, and Ron Kimmel. Surface reconstruction from gaussian splatting via novel stereo views. *arXiv preprint arXiv:2404.01810*, 2024. 2

[56] Tong Wu, Jiaqi Wang, Xingang Pan, Xudong Xu, Christian Theobalt, Ziwei Liu, and Dahua Lin. Voxurf: Voxel-based efficient and accurate neural surface reconstruction. *arXiv preprint arXiv:2208.12697*, 2022. 2, 4

[57] Tong Wu, Jiarui Zhang, Xiao Fu, Yuxin Wang, Liang Pan Jiawei Ren, Wayne Wu, Lei Yang, Jiaqi Wang, Chen Qian, Dahua Lin, and Ziwei Liu. Omniobject3d: Large-vocabulary 3d object dataset for realistic perception, reconstruction and generation. In *IEEE/CVF Conference on Computer Vision and Pattern Recognition (CVPR)*, 2023. 5

[58] Haodong Xiang, Xinghui Li, Xiansong Lai, Wanting Zhang, Zhichao Liao, Kai Cheng, and Xueping Liu. Gaussianroom: Improving 3d gaussian splatting with sdf guidance and monocular cues for indoor scene reconstruction. *arXiv preprint arXiv:2405.19671*, 2024. 3

[59] Baixin Xu, Jiarui Zhang, Kwan-Yee Lin, Chen Qian, and Ying He. Deformable model-driven neural rendering for high-fidelity 3d reconstruction of human heads under low-view settings. In *Proceedings of the IEEE/CVF International Conference on Computer Vision*, pages 17924–17934, 2023. 2, 4

[60] Baixin Xu, Jiangbei Hu, Fei Hou, Kwan-Yee Lin, Wayne Wu, Chen Qian, and Ying He. Parameterization-driven neural surface reconstruction for object-oriented editing in neural rendering. 2024. 1

[61] Rui Xu, Zhiyang Dou, Ningna Wang, Shiqing Xin, Shuangmin Chen, Mingyan Jiang, Xiaohu Guo, Wenping Wang, and Changhe Tu. Globally consistent normal orientation for point clouds by regularizing the winding-number field. *ACM Trans. Graph.*, 42(4), 2023. 2

[62] Lior Yariv, Yoni Kasten, Dror Moran, Meirav Galun, Matan Atzmon, Basri Ronen, and Yaron Lipman. Multiview neural surface reconstruction by disentangling geometry and appearance. In *Advances in Neural Information Processing Systems*, pages 2492–2502, 2020. 5

[63] Lior Yariv, Jiatao Gu, Yoni Kasten, and Yaron Lipman. Volume rendering of neural implicit surfaces. In *Advances in Neural Information Processing Systems*, pages 4805–4815, 2021. 1, 2, 4, 5, 6, 7

[64] Mulin Yu, Tao Lu, Linning Xu, Lihan Jiang, Yuanbo Xiangli, and Bo Dai. Gsdf: 3dgs meets sdf for improved rendering and reconstruction. *arXiv preprint arXiv:2403.16964*, 2024. 1, 3, 5

[65] Zehao Yu, Torsten Sattler, and Andreas Geiger. Gaussian opacity fields: Efficient and compact surface reconstruction in unbounded scenes. *arXiv preprint arXiv:2404.10772*, 2024. 2, 3, 5, 6, 7, 1

[66] Fangneng Zhan, Lingjie Liu, Adam Kortylewski, and Christian Theobalt. General neural gauge fields. *arXiv preprint arXiv:2305.03462*, 2023. 1

[67] Chen Zhang, Wanjuan Su, and Wenbing Tao. Point-neus: Point-guided neural implicit surface reconstruction by volume rendering. *arXiv preprint arXiv:2310.07997*, 2023. 1

[68] Haoran Zhang, Junkai Deng, Xuhui Chen, Fei Hou, Wencheng Wang, Hong Qin, Chen Qian, and Ying He. From transparent to opaque: Rethinking neural implicit surfaces with α-neus. In *Advances in Neural Information Processing Systems (NeurIPS)*, 2024. 5, 8

[69] Jingyang Zhang, Yao Yao, Shiwei Li, Jingbo Liu, Tian Fang, David McKinnon, Yanghai Tsin, and Long Quan. Neilf++: Inter-reflectable light fields for geometry and material estimation. In *Proceedings of the IEEE/CVF International Conference on Computer Vision*, pages 3601–3610, 2023. 1

[70] Weixing Zhang, Zongrui Li, De Ma, Huajin Tang, Xudong Jiang, Qian Zheng, and Gang Pan. Spiking gs: Towards high-accuracy and low-cost surface reconstruction via spiking neuron-based gaussian splatting. *arXiv preprint arXiv:2410.07266*, 2024. 2

[71] Wenyuan Zhang, Yu-Shen Liu, and Zhizhong Han. Neural signed distance function inference through splatting 3d gaussians pulled on zero-level set. *arXiv preprint arXiv:2410.14189*, 2024. 3

[72] Xiuming Zhang, Pratul P Srinivasan, Boyang Deng, Paul Debevec, William T Freeman, and Jonathan T Barron. Nerfactor: Neural factorization of shape and reflectance under an unknown illumination. *ACM Transactions on Graphics (ToG)*, 40(6):1–18, 2021. 1

[73] Yufeng Zheng, Wang Yifan, Gordon Wetzstein, Michael J Black, and Otmar Hilliges. Pointavatar: Deformable point-based head avatars from videos. In *Proceedings of the IEEE/CVF conference on computer vision and pattern recognition*, pages 21057–21067, 2023. 1

GSurf: 3D Reconstruction via Signed Distance Fields with Direct Gaussian Supervision

Supplementary Material

6. Implementation details

We disable the sigmoid activation function in appearance modeling, as we observed that it may hinder the gradients of screen points in terms of densification and splitting.

GaussianSurfels [11] employs Poisson reconstruction for mesh extraction, which often takes over half an hour for mesh extraction and refinement, particularly when dealing with a large number of points. We noted that GOF [65] evaluates Chamfer distance using meshes generated from the TSDF for the DTU dataset [20] in its official script. Therefore, we visualize the TSDF results in the main paper and supplementary materials for a more comprehensive comparison.

7. Additional results

We provide the remaining results for the DTU dataset [20] in Fig. 8 and Fig. 9. We also report rendering results on the OmniObjects-d dataset, where the images for each object are split with a training-to-evaluation ratio of 8:1. We evaluate performance using PSNR, SSIM, and LPIPS metrics on novel view images (see Tab. 4). Our findings show that 2DGS achieves approximately 40 dB PSNR, benefiting form the availability of sufficient training images (approximately 80–90 per object). In contrast, our method observes a slight reduction of about 1 dB, attributable to the constraints imposed on the Gaussians. Nevertheless, for more challenging objects with complex geometries or varying lighting conditions, our method demonstrates greater robustness compared to 2DGS, owing to its more accurate geometry reconstruction.

Fig. 10 shows our geometry reconstruction on scene-level data. While SDF-based methods often struggle with large-scale scene reconstruction due to scene complexity and sparse input data, our approach achieves smooth results.

One limitation of our method is its reliance on Gaussian centroids as keypoints. Under sparse-view conditions or in challenging scenarios, such as reflective surfaces, the Gaussians may be generated sparsely or inaccurately, compromising the quality of the reconstructed geometry.

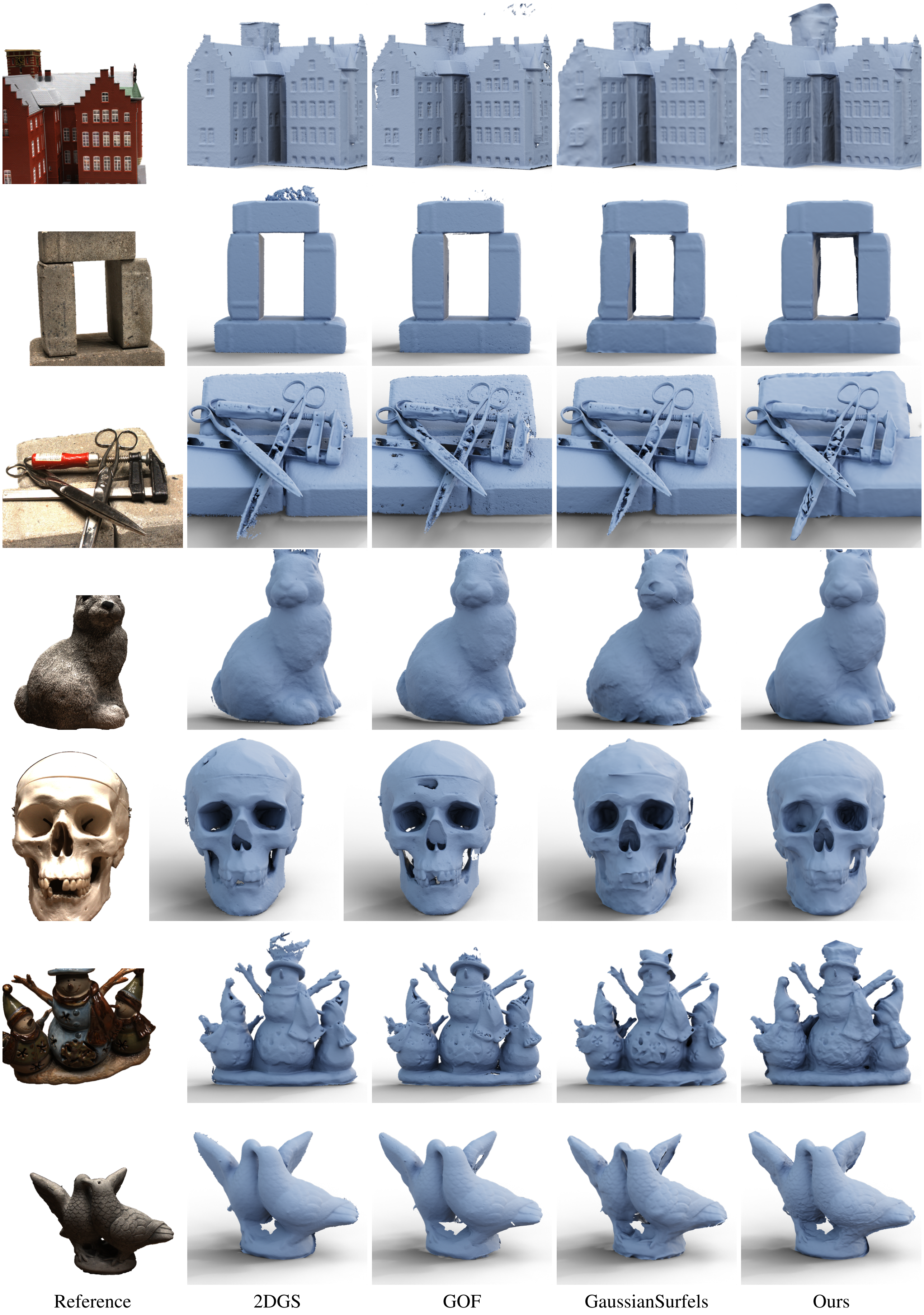

Figure 8. Visual results on the rest of the DTU dataset. We present visualizations of the culled meshes after applying cropping, using the scripts from 2DGS [19] and GOF [65].

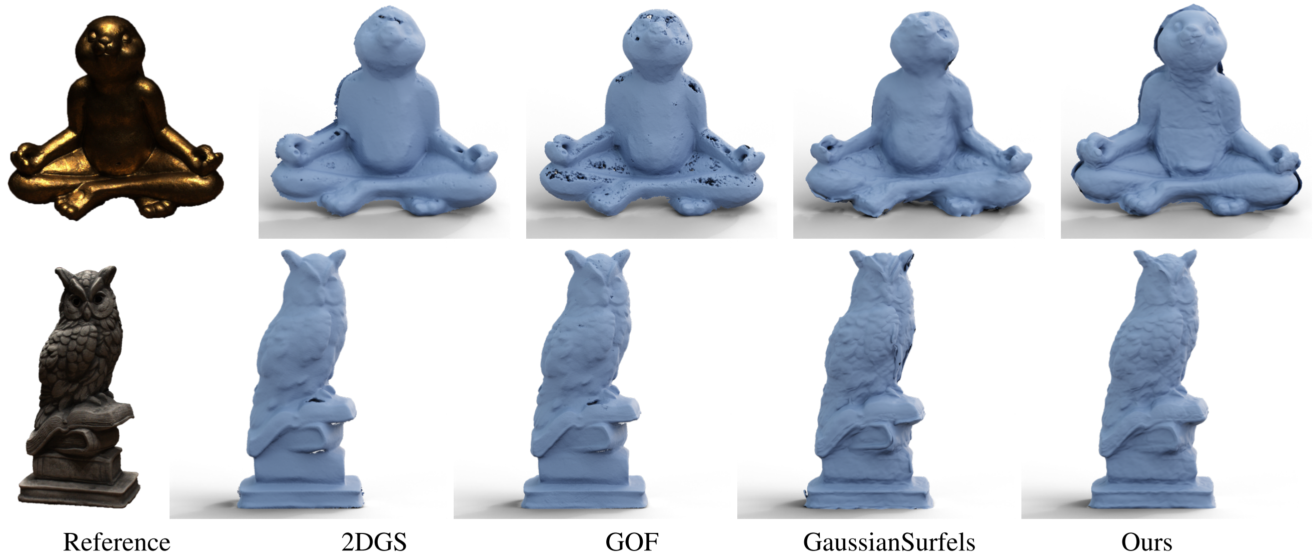

Figure 9. Visual results on the rest of the DTU dataset. We present visualizations of the culled meshes after applying cropping, using the scripts from 2DGS [19] and GOF [65].

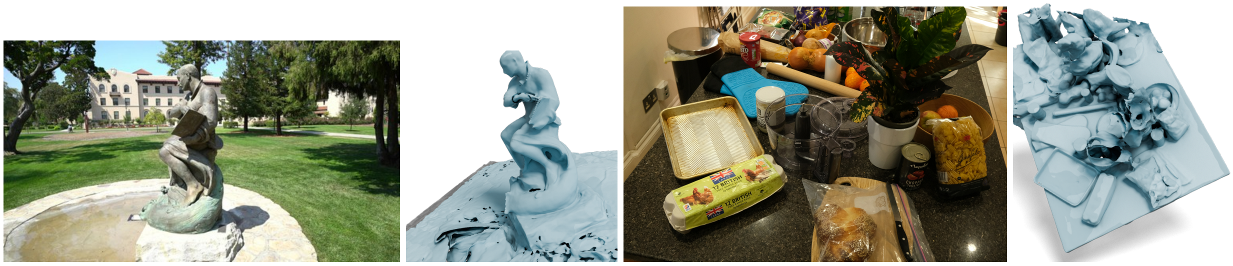

Figure 10. Scene reconstruction from the Tanks and Temples dataset [27] and the MipNeRF360 dataset [4].

Table 4. Quantitative evaluation (PSNR ↑, SSIM ↑, and LPIPS ↓) for novel view synthesis on the OmniObjects3D-d dataset.

Method	Ornaments															Antique								
	1			3			4			5			8			16			19			21		
	PSNR	SSIM	LPIPS	PSNR	SSIM	LPIPS	PSNR	SSIM	LPIPS	PSNR	SSIM	LPIPS	PSNR	SSIM	LPIPS	PSNR	SSIM	LPIPS	PSNR	SSIM	LPIPS	PSNR	SSIM	LPIPS
2DGS [19]	39.52	0.994	0.014	42.37	0.996	0.015	41.00	0.995	0.017	40.76	0.996	0.010	40.87	0.991	0.018	31.84	0.854	0.121	34.05	0.943	0.061	36.14	0.956	0.056
Ours	38.63	0.993	0.018	38.97	0.992	0.028	40.24	0.994	0.024	39.95	0.994	0.014	41.64	0.989	0.023	40.30	0.981	0.077	36.59	0.973	0.033	44.17	0.992	0.027